Supporting Information

Origin of High Efficiencies for Thermally Activated Delayed Fluorescence OLEDs: Atomistic Insight into Molecular Orientation and Torsional Disorder

Taiping Hu,[ab] Guangchao Han,[a] Zeyi Tu,[ab] Ruihuong Duan, [ab] and Yuanping Yi*[ab]

[a] CAS Key Laboratory of Organic Solids, CAS Research/Education Center for Excellence in Molecular Sciences, Institute of Chemistry, Chinese Academy of Sciences, Beijing 100190, China
[b] University of Chinese Academy Sciences, Beijing, 100049, China

Simulation and Computational Details

1. Force field validation

The bonded and non-bonded interaction parameters of mCPCN, DMAC-TRZ and mCP were built from the general Amber force field (GAFF).[1] The missing bonded parameters for mCPCN and mCP were taken from the work reported by Muccioli et al.[2] The RESP charges were used as partial charges.[3] Firstly, the force field parameters were validated by comparing the MM-optimized molecular geometries with the geometries obtained by DFT or MP2 methods and the X-ray crystallographic geometry. The results indicate that the GAFF can well reproduce the experimental and quantum-chemistry geometries (see Figure S1 and Tables S1-S4).[4]

Subsequently, isothermal-isobaric (NPT) MD simulations were performed on a 5×5×5 supercell for the mCP crystal. The supercell was equilibrated for 2.5 ns. In the simulations, a time step of 1 fs was set for the leap-frog integrator and the temperature of 300 K and pressure of 1 atm were maintained by the Berendsen thermostat and barostat, respectively. A cutoff of 1.2 nm for the summation of van der Waals interaction and Particle-Mesh Ewald solver for long-range Coulomb interactions were used in the simulations. The results point to that the lattice parameters obtained by MD simulations with the GAFF are in good agreement with the experimental results (see Table S2).[4]

2. Vapor deposition

2.1 Substrates construction

The initial substrates were constructed by cleaving the mCP crystal along the (100), (010), and (001) crystallographic planes, respectively. To construct slab models for deposition, the unit cell was replicated to build 8×5×3, 6×10×3, 10×8×2 supercells for the (100), (010) and (001) substrate surfaces, respectively. The z-direction lattice of each slab was elongated to about 20 nm to form a vacuum layer for deposition. These supercells were then fully equilibrated at room temperature (300 K) using the NVT ensemble and three-dimension periodic boundary condition. The molecules in the middle layer of the substrate remain stable during thermal relaxation, indicating that

the thickness (ca. 5.0 nm) of those slabs is large enough.

2.2 Vapor deposition process

The vapor-phase deposition process is similar to that used previously by Muccioli et al and by our group.[5-6] One host or emitter molecule was deposited every 100 ps within a 2 nm height from the top of the relaxed substrate or previously deposited molecules. This process was repeated until a total of 1500 emitter and host molecules were deposited to form a final thin film. Since the deposited molecules only interact with the surface molecules of the substrate but have little influence on the bottom molecule, the positions of the molecules in the bottom layer of the substrate were frozen while the other substrate molecules and deposited molecules were allowed to fully relax in the MD simulations. Each step of the deposition was carried out at 400 K using the leap-frog integrator under the canonical (NVT) ensemble employing the V-rescale thermostat and time step of 1 fs. A cutoff of 1.2 nm was used for the summation of van der Waals (vdW) interaction and the particle-mesh Ewald (PME) approach for long-range Coulomb interaction. The final thin films were generated with the emitter:host mole ratio of nearly 1:9, corresponding to the 12% weight concentration for the emitter. After deposition of all molecules, the system was fully relaxed under the NVT ensemble at 400 K for 10 ns, then annealed to 300 K within 2.5 ns, and finally equilibrated at 300 K for 15 ns with the last 10 ns used to extract the data for analysis.

3. High temperature annealing

We also simulated the blending morphology of host and emitter molecules via high temperature annealing (i.e., without substrate) by the following steps (see Figure S2): (i) randomly placing 1500 molecules (the mole ratio of emitter vs host is nearly 1:9, corresponding to 12 wt% doped concentration) into a large box ($25\times25\times25$ nm^3) to generate an initial model using the Packmol package[7] (seeding); (ii) performing NPT simulation for 5 ns under 600 K and 100 bar to make molecules close together (compression); (iii) equilibration under 600 K and 1 bar for 10 ns, then cooling from 600 K down to 300 K gradually within 3 ns (thermal annealing); (iv) equilibration at

300 K and 1 bar for 20 ns (equilibration). Five independent samples were simulated for statistical analysis. The final box size is ca. 10.28 nm in three dimensions.

4. Surface energy

Surface energy is an important parameter for measuring the surface stabilities of materials.[8-10] It can be evaluated by using the total energy of the slab (E_S) and the supercell (E_T) according to the following equation:

$$E = \left(E_S - E_T\right)/2A \tag{S1}$$

where A is the cross-sectional area of the surface. The values of E_S and E_T can be obtained via EM or MD simulations. For simplicity, the slab and supercell should have the same number of molecules.

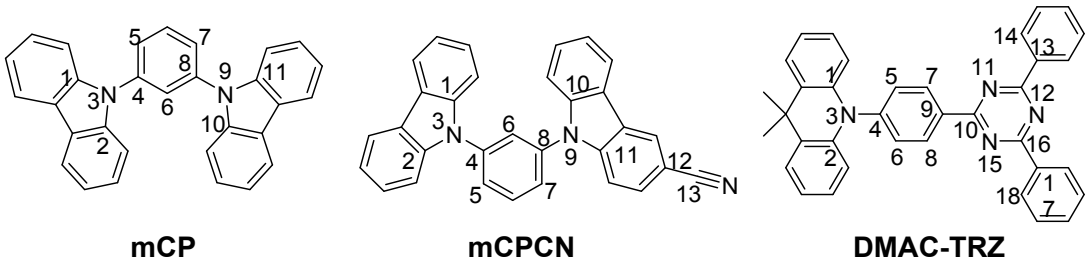

Figure S1. Illustration of bonds, angles, and dihedrals used for comparison in mCP, mCPCN, and DMAC-TRZ.

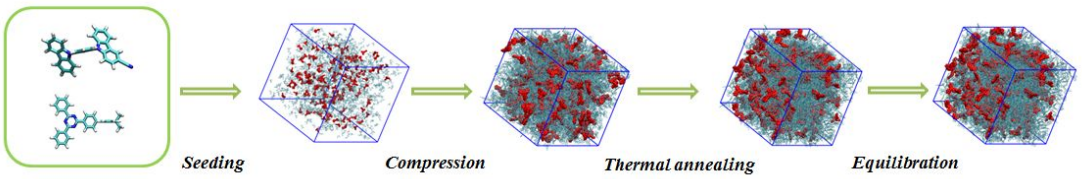

Figure S2 Workflow of simulating the blending morphologies by high temperature annealing. Red vdW and transparent licorice drawings represent DMAC-TRZ and mCPCN, respectively.

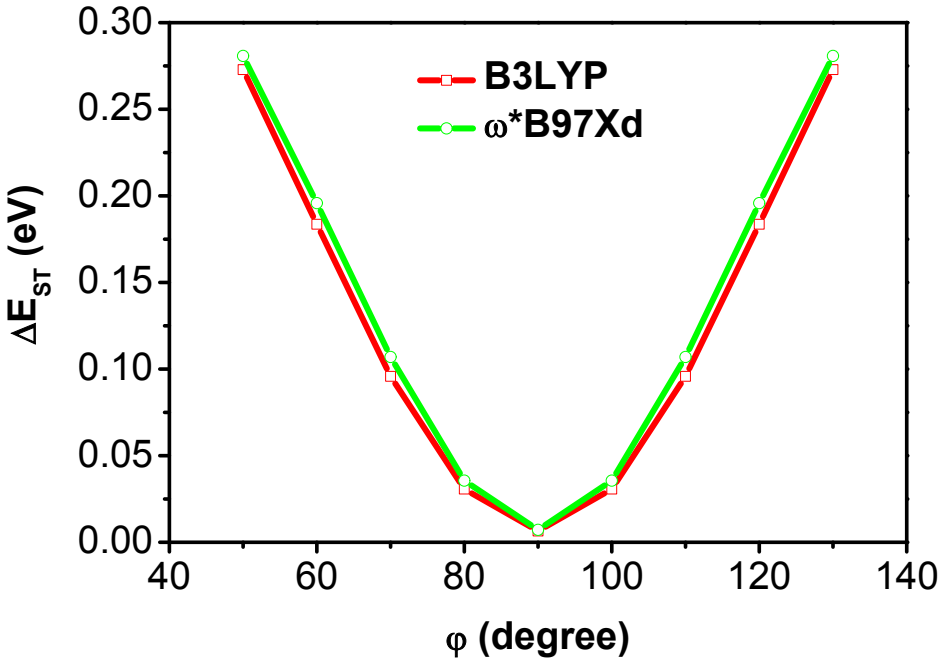

Figure S3. TDDFT-calculated energy difference between S_1 and T_1 (ΔE_{ST}) as a function of the torsion angle (φ) between the electron-donating and electron-withdrawing units for DMAC-TRZ.

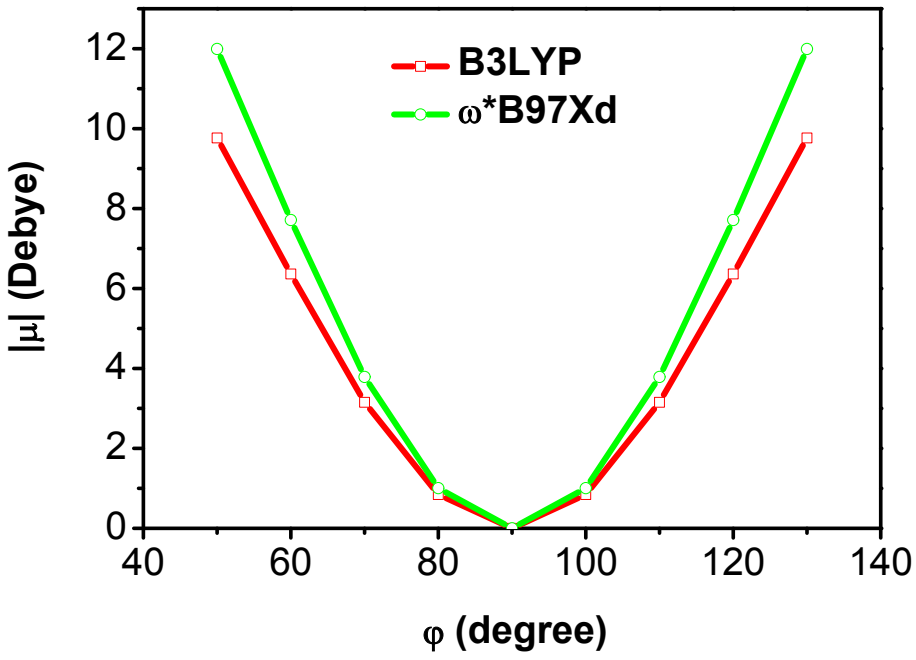

Figure S4. TDDFT-calculated transition dipole moment (μ) as a function of the torsion angle (φ) between the electron-donating and electron-withdrawing units for DMAC-TRZ.

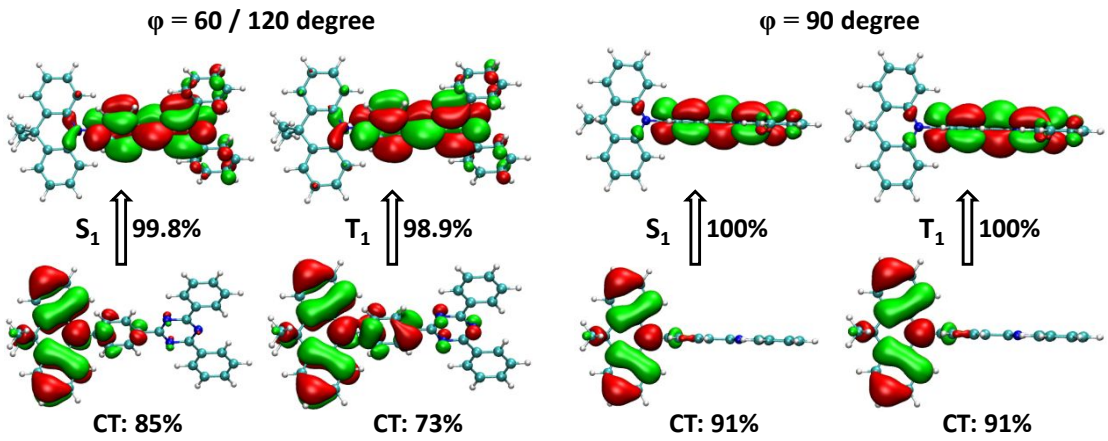

Figure S5. TDDFT-B3LYP/6-31G**-calculated natural transition orbitals (lower: hole, upper: electron) for the $S_0 \rightarrow S_1$ and $S_0 \rightarrow T_1$ excitations based on the geometric structures with the torsion angle of 90º and 60º or 120º. CT components are also listed.

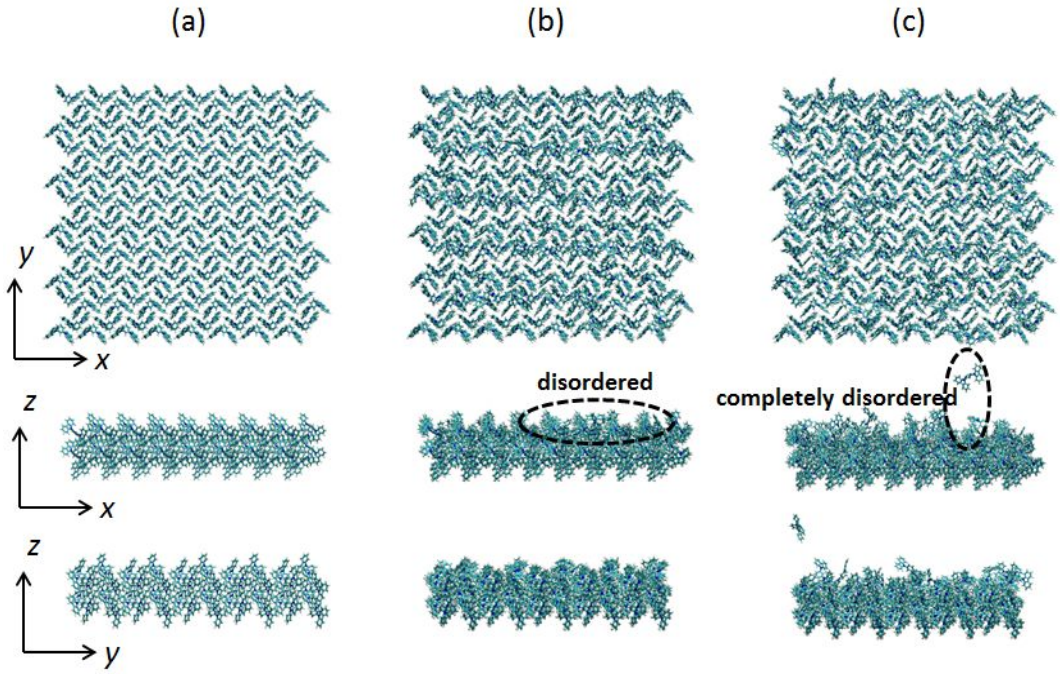

Figure S6. Top and side views of the upper layers of the (100) surface: (a) initial structure; (b) after EM and 2.5 ns equilibration (NVT); (c) after deposition of host and emitter molecules.

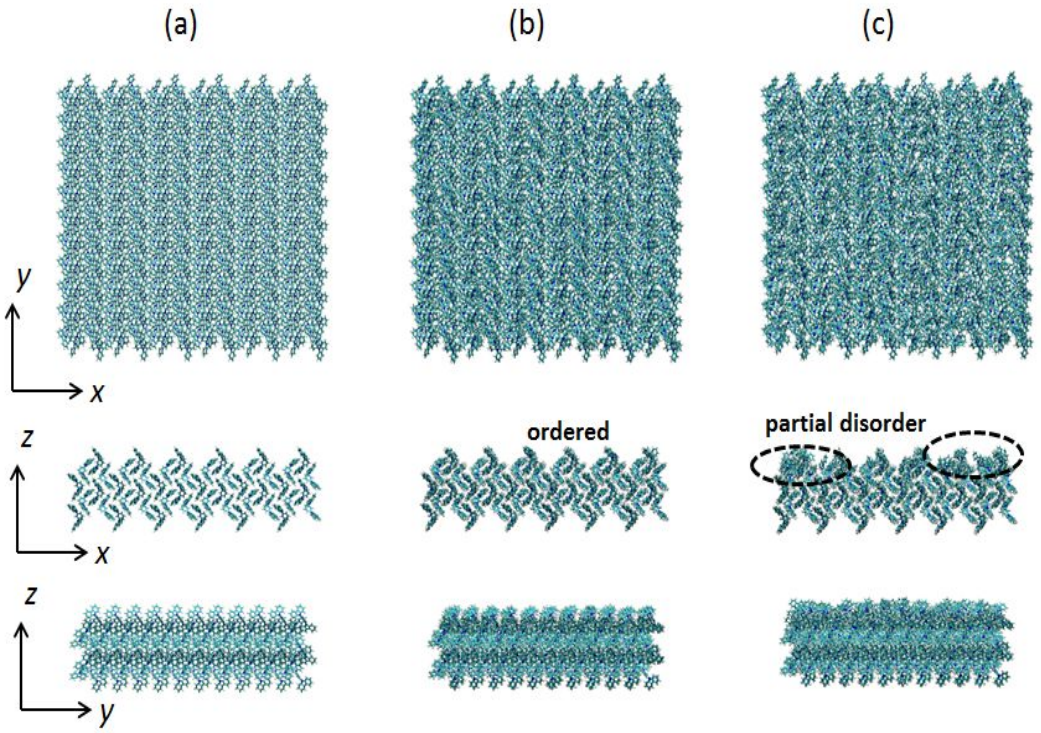

Figure S7. Top and side views of the upper layers of the (010) surface: (a) initial structure; (b) after EM and 2.5 ns equilibration (NVT); (c) after depositions of host and emitter molecules.

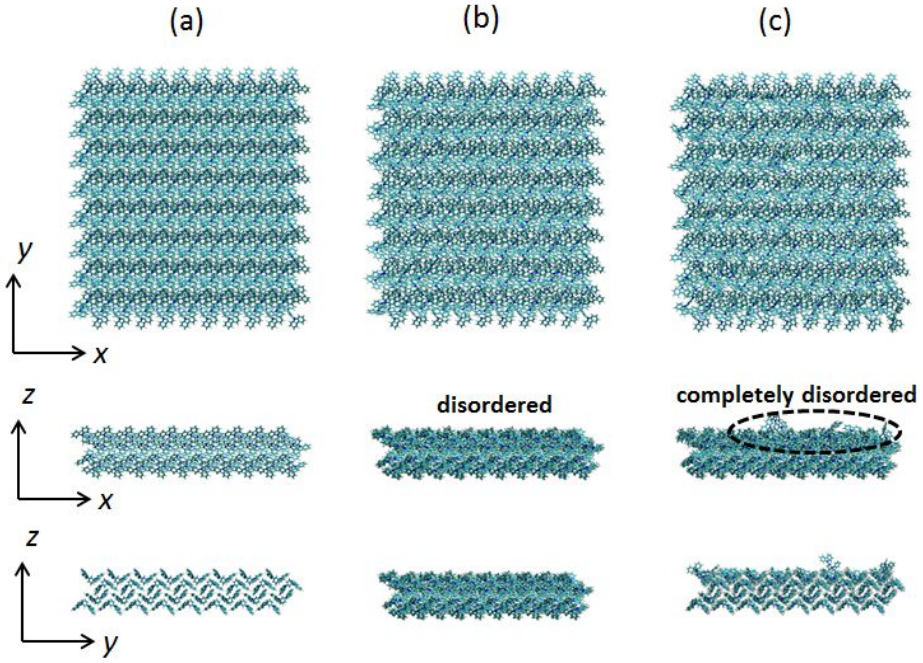

Figure S8. Top and side views of the upper layers of the (001) surface: (a) initial structure; (b) after EM and 2.5 ns equilibration (NVT); (c) after depositions of host and emitter molecules.

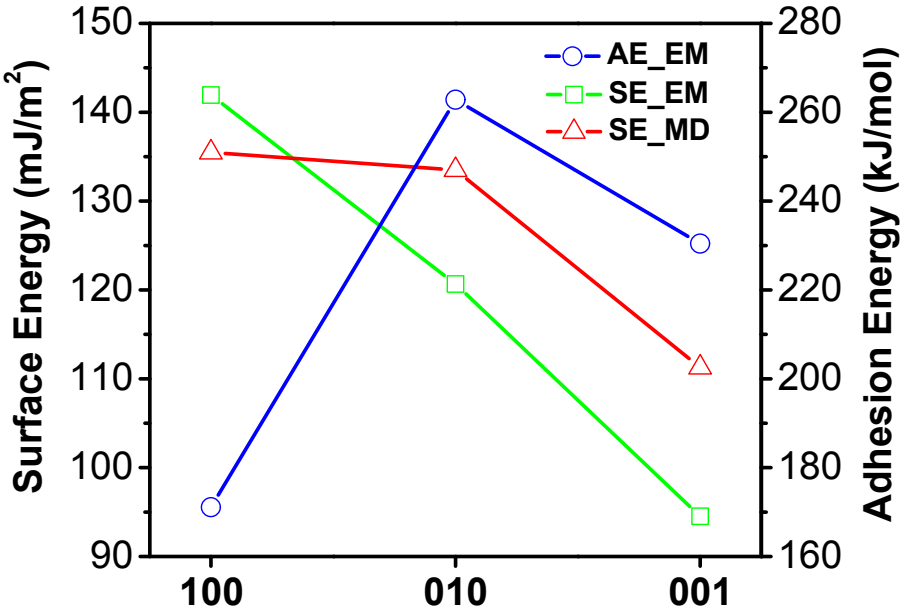

Figure S9. Calculated surface energies (SE) via energy minimization (EM) and NVT equilibration and adhesion energies (AE) via EM for the studied mCP surfaces.

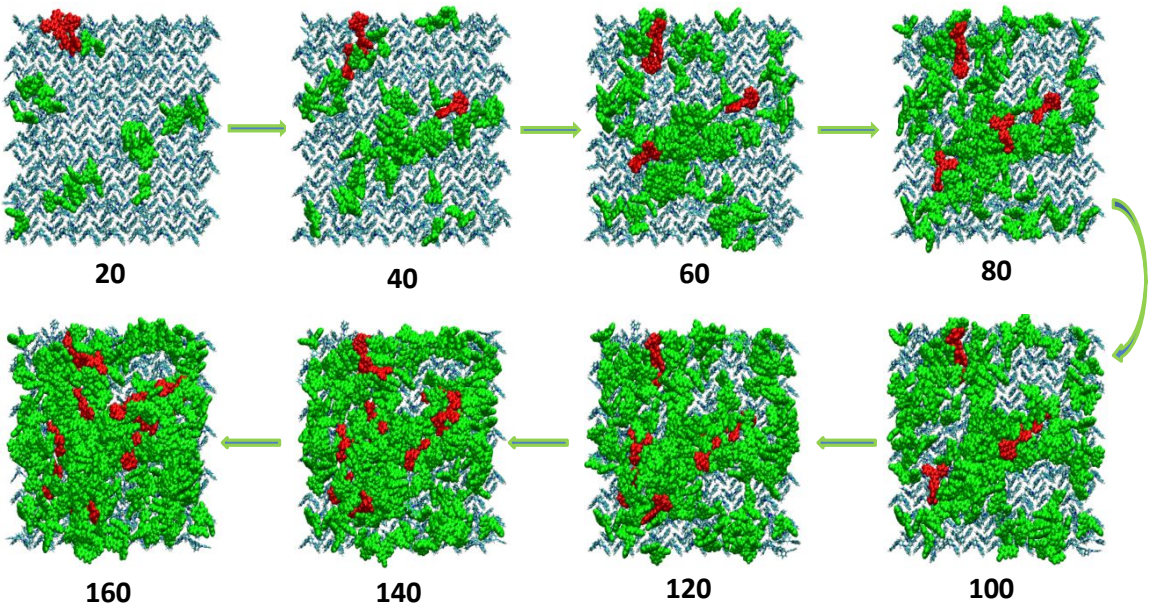

Figure S10. Evolutions of molecular sites on the (100) surface at the early deposition stage. The number of deposited host and emitter molecules is shown. Red and green colors represent the emitter and host molecules, respectively.

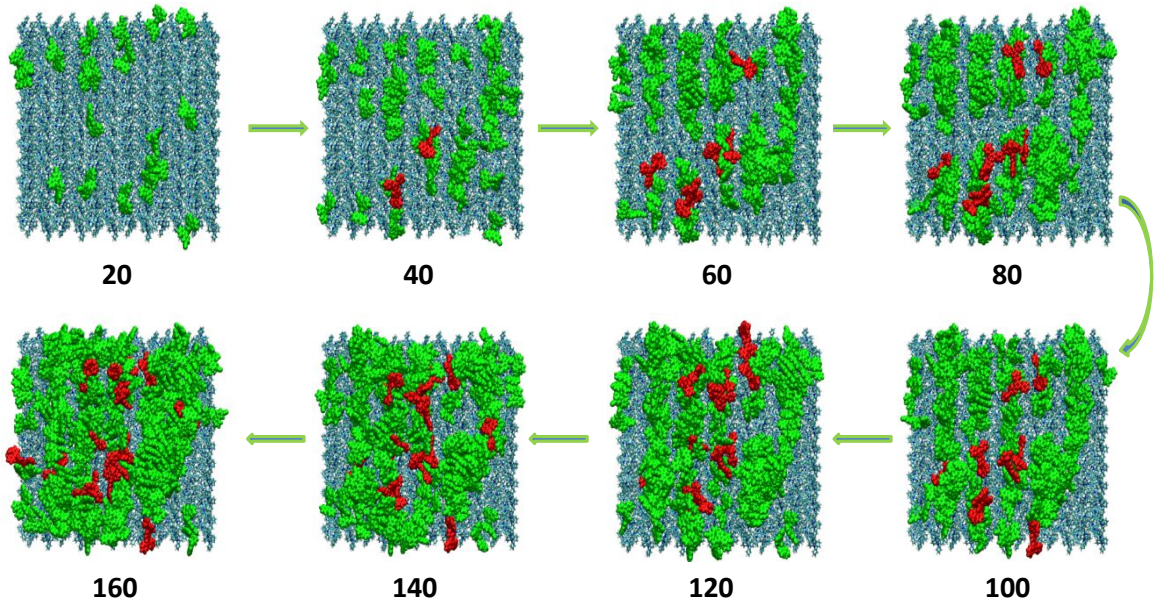

Figure S11. Evolutions of molecular sites on the (010) surface at the early deposition stage. The number of deposited host and emitter molecules is shown. Red and green colors represent the emitter and host molecules, respectively.

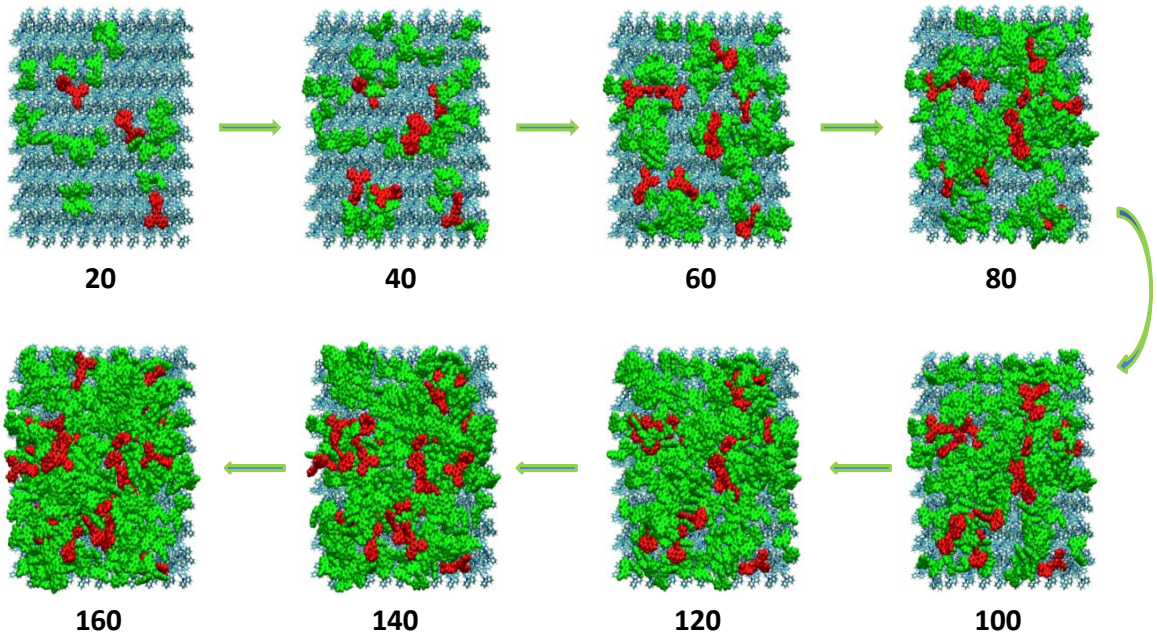

Figure S12. Evolutions of molecular sites on the (001) surface at the early deposition stage. The number of deposited host and emitter molecules is shown. Red and green colors represent the emitter and host molecules, respectively.

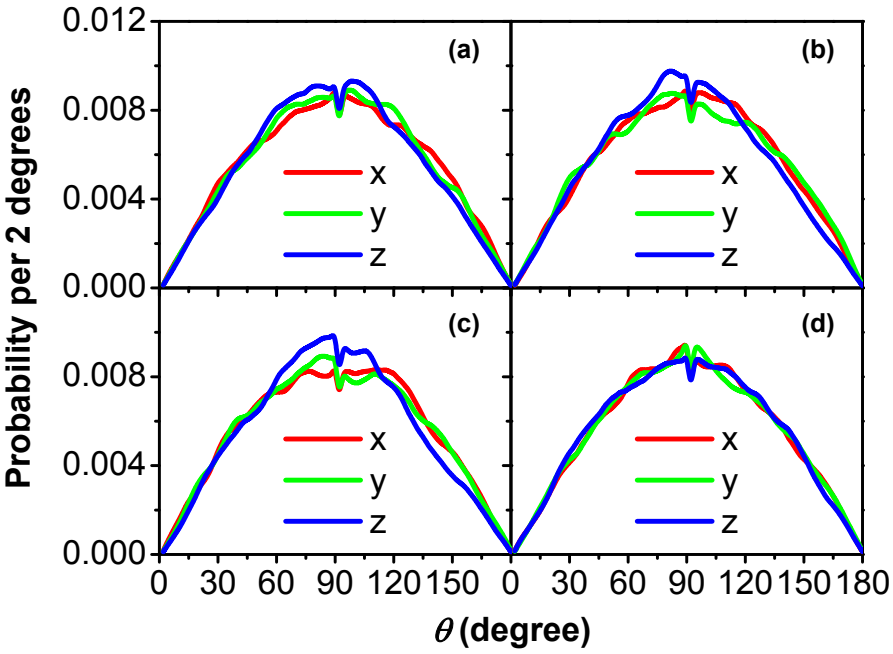

Figure S13. Distributions of the angles from the host A2 axis to the coordinate axes for the deposited films on (a) the (100) surface, (b) the (010) surface, and (c) the (001) surface as well as (d) the blending mixture obtained by high temperature annealing. The z-direction corresponds to the substrate normal direction.

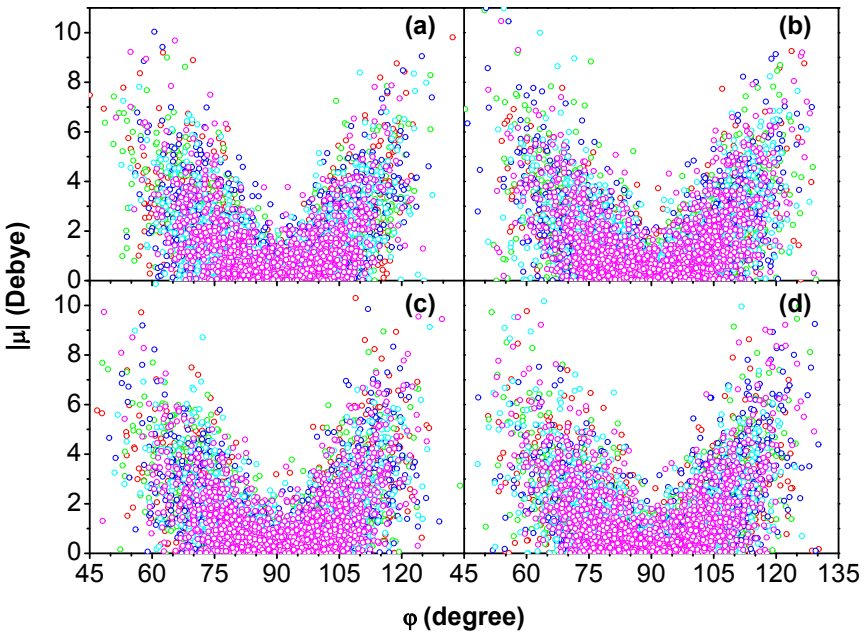

Figure S14. Scatter plots of the transition dipole moments (μ) vs the torsion angles (φ) between the electron-donating and electron-withdrawing units for the emitter molecules extracted from the deposited films on (a) the (100) surface, (b) the (010) surface, and (c) the (001) surface as well as (d) the blending mixture obtained by high temperature annealing. Five samples are represented by different colors.

Table S1. Comparison of selected bond lengths, bond angles, and dihedral angles for an isolated mCP molecule optimized by MM, DFT, and MP2 methods as well as measured by X-ray diffraction.[4]

Bond length (Å)

	1-3	2-3	3-4	8-9	9-10	9-11
GAFF	1.40	1.40	1.39	1.39	1.40	1.40
DFT	1.40	1.40	1.42	1.42	1.40	1.40
MP2	1.39	1.39	1.41	1.41	1.39	1.39
Exp.	1.39	1.40	1.43	1.42	1.40	1.41

Bond angle (degree)

	1-3-2	1-3-4	2-3-4	3-4-5	3-4-6	6-8-9	7-8-9	8-9-10	8-9-11	10-9-11
GAFF	112.1	123.9	123.8	120.8	119.3	119.3	120.8	123.8	123.9	112.1
DFT	108.4	125.7	125.9	120.2	119.9	119.9	120.2	125.9	125.7	108.4
MP2	108.8	125.5	125.7	119.9	119.5	119.5	119.9	125.7	125.5	108.8
Exp.	108.7	124.3	126.5	119.2	119.9	120.4	119.9	125.8	125.6	108.4

Dihedral angle (degree)

	1-3-4-5	6-8-9-10
GAFF	51.6	59.5
DFT	54.7	54.1
MP2	53.4	51.4
Exp.	62.1	43.4

Table S2. Lattice parameters of a unit cell for mCP obtained by NPT simulations with the GAFF compared with the experimental measurement.[4]

	Exp.	GAFF	Deviation
a (Å)	9.07	9.13	0.66%
b (Å)	12.50	12.58	0.64%
c (Å)	19.04	19.16	0.63%

Table S3. Comparison of selected bond lengths, bond angles and dihedral angles for an isolated mCPCN molecule optimized by MM, DFT, and MP2 methods.

Bond length (Å)

	1-3	2-3	3-4	8-9	9-10	9-11	12-13
GAFF	1.41	1.41	1.40	1.41	1.41	1.41	1.44
DFT	1.40	1.40	1.42	1.42	1.40	1.39	1.43
MP2	1.39	1.40	1.41	1.41	1.39	1.39	1.43

Bond angle (degree)

	1-3-2	1-3-4	2-3-4	3-4-5	3-4-6	6-8-9	7-8-9	8-9-10	8-9-11	10-9-11
GAFF	106.7	126.7	126.8	120.4	120.3	120.3	119.9	126.7	126.6	106.8
DFT	108.4	125.7	125.9	120.3	119.9	119.7	120.1	125.8	125.6	108.6
MP2	108.8	125.5	125.7	120.0	119.6	119.4	119.8	125.7	125.5	108.8

Dihedral angle (degree)

	1-3-4-6	6-8-9-10
GAFF	123.5	60.5
DFT	123.0	61.9
MP2	127.8	53.0

Table S4. Comparison of selected bond lengths and dihedral angles for an isolated DMAC-TRZ molecule optimized by MM, DFT, and MP2 methods.

Bond length (Å)

	1-3	2-3	3-4	9-10	12-13	16-17
GAFF	1.37	1.36	1.35	1.43	1.43	1.43
DFT	1.40	1.40	1.43	1.48	1.48	1.48
MP2	1.40	1.40	1.42	1.48	1.48	1.48

Dihedral angle (degree)

	1-3-4-5	7-9-10-11	11-12-13-14	15-16-17-18
GAFF	92.6	0.4	0.0	0.5
DFT	90.0	0.0	0.0	0.0
MP2	90.0	0.0	0.0	0.0

References

1. J. Wang; R. M. Wolf; J. W. Caldwell; P. A. Kollman; Case, D. A., Development and Testing of a General Amber Force Field. *J. Comput. Chem* **2004,** *25* (9), 1157-1174.
2. Moral, M.; Son, W. J.; Sancho-Garcia, J. C.; Olivier, Y.; Muccioli, L., Cost-Effective Force Field Tailored for Solid-Phase Simulations of OLED Materials. *J. Chem. Theory Comput.* **2015,** *11* (7), 3383-3392.
3. Christopher I. Bayly, P. C., Wendy D. Cornell, and Peter A. Kollman, A Well-Behaved Electrostatic Potential Based Method Using Charge Restraints for Deriving Atomic Charges: The RESP Model. *J. Phys. Chem.* **1993,** *97*, 10269-10280.
4. Sun, Y.-H.; Zhu, X.-H.; Chen, Z.; Zhang, Y.; Cao, Y., Potential Solution Processible Phosphorescent Iridium Complexes toward Applications in Doped Light-Emitting Diodes: Rapid Syntheses and Optical and Morphological Characterizations. *J. Org. Chem* **2006,** *71* (16), 6281-6284.
5. Muccioli, L.; D'Avino, G.; Zannoni, C., Simulation of vapor-phase deposition and growth of a pentacene thin film on C60 (001). *Adv. Mater.* **2011,** *23* (39), 4532-4536.
6. Han, G.; Shen, X.; Yi, Y., Deposition Growth and Morphologies of C60on DTDCTB Surfaces: An Atomistic Insight into the Integrated Impact of Surface Stability, Landscape, and Molecular Orientation. *Adv. Mater. Interfaces* **2015,** *2* (17), 1500329.
7. Martinez, L.; Andrade, R.; Birgin, E. G.; Martinez, J. M., PACKMOL: a package for building initial configurations for molecular dynamics simulations. *J. Comput. Chem.* **2009,** *30* (13), 2157-2164.
8. Fu, Y. T.; Risko, C.; Bredas, J. L., Intermixing at the pentacene-fullerene bilayer interface: a molecular dynamics study. *Adv. Mater.* **2013,** *25* (6), 878-882.
9. Mauger, S. A.; Chang, L.; Friedrich, S.; Rochester, C. W.; Huang, D. M.; Wang, P.; Moulé, A. J., Self-Assembly of Selective Interfaces in Organic Photovoltaics. *Adv. Funct. Mater.* **2013,** *23* (15), 1935-1946.
10. Tummala, N. R.; Mehraeen, S.; Fu, Y.-T.; Risko, C.; Brédas, J.-L., Materials-Scale Implications of Solvent and Temperature on [6,6]-Phenyl-C61-butyric Acid Methyl Ester (PCBM): A Theoretical Perspective. *Adv. Funct. Mater.* **2013,** *23* (46), 5800-5813.